

Constitutive Modeling of Liver Tissue: Experiment and Theory*

Zhan Gao[†], Kevin Lister and Jaydev P. Desai, *Senior Member, IEEE*
Robotics, Automation, Manipulation, and Sensing (RAMS) Laboratory
University of Maryland, College Park, MD, USA
E-mail: {zgao@umd.edu, klistler@umd.edu, jaydev@umd.edu}

Abstract—Mechanical models for soft organ tissues are necessary for a variety of medical applications, such as surgical planning, virtual reality surgery simulators, and for diagnostic purposes. An adequate quantitative description of the mechanical behavior of tissues requires adequate and accurate experimental data to be acquired and analyzed. We present results of three types of ex vivo tests on pig liver tissue, i.e. simple tension, unconfined compression and pure shear. A new constitutive model based on combined logarithmic and Ogden strain energy is proposed. The model accounts very well for observed non-linear stress-strain relations for full strain range of tension and compression and represents equally well the mechanical response of pure shear when strain is less than 35%.

I. INTRODUCTION

A biomechanical model of soft tissue derived from experimental measurements is critical for developing a reality-based model for minimally invasive surgical training and simulation. In our research, we have been focusing on developing a biomechanical model of the liver with the ultimate goal of using this model for local tool-tissue interaction tasks and providing feedback to the surgeon through a haptic display.

The mechanical properties of ‘very’ soft tissues, i.e., tissues that do not bear mechanical loads (brain, liver, kidney, etc.), have only been extensively investigated over the last decade [1-6]. Most of the reported models for soft tissues under large deformation are based on certain type of strain energy function, and many are derived from compressive loading experiments. Miller and Chinzei [1] proposed a constitutive equation of polynomial form with time-dependent coefficients to describe swine brain tissue in compression. Davies et al [7] derived exponential stress-strain law according to the indentation tests on spleen tissue. Roan and Vemaganti [8] conducted no-slip uniaxial compression on bovine liver tissue; exponential form of strain energy and finite element simulation were used to determine the material properties. Miller and Chinzei [9] were one of the first to study very soft tissue properties in tension. They proposed a viscoelastic model based on the generalization of the Ogden strain energy for brain tissue with strain up to 30% in compression and 60% in tension. In Nava et.al [10] aspiration experiments, the liver tissue was

mainly in tension. The reduced polynomial form of strain energy and quasi-linear viscoelastic model was used for the inverse finite element simulation to determine the mechanical properties[11]. Chui et al [12] proposed a new constitutive formulation that combined logarithmic and polynomial strain energy in modeling the combined compression and elongation experiments. The modeled strain range was up to 40% in compression and 60% in tension. Since the logarithmic form of strain energy function was used, it was possible to represent the dramatic increase of stress after the initial low stiffness toe region in the stress strain curve.

The concept of pseudo-elasticity for bio-tissues was proposed by Fung [13]. Fung states that as long as the stress-strain relationship of a bio-tissue is well defined, repeatable and predictable under certain conditions (such as in preconditioned tissue), we can treat the material under that particular condition as an elastic material. Thus the techniques of elasticity theory can be borrowed to handle an inelastic material. The most often used concept in pseudo-elasticity is the assumption that a strain energy function exists. Although only an approximation, the use of strain energy function for soft tissues is very convenient, because the multi-axial stress-strain relationships can be derived directly from the strain energy. Since for a general surgical simulation, various loading states may be involved, to define a realistic strain energy would require characterization of soft-tissue in various deformation modes.

In this paper, we present results of simple tension, unconfined compression, and pure shear tests for ex-vivo pig liver tissue undergoing finite deformation. To eliminate or minimize the strain rate effect, all the experiments were conducted at the same low speed, namely, 1.3 mm/s. The results showed that liver tissue behavior in one deformation mode is considerably different from its behavior in other modes; therefore, tissue constitutive models based on only one type of experiments are not suitable for description of tissue behavior in general. The two previous models based on both tension and compression tests are not adequate to fit our results: Ogden’s model [9] cannot represent the dramatic increase of stress after the toe region while Chui et. al.’s model is hard to use if the tissue’s stiffness in tension is much softer than that predicted in that particular model. After rigorous mathematical description of the theoretical framework, we propose a new constitutive model based on a combined logarithmic-Ogden energy function. We demonstrate that the proposed model describes well the liver

*This work was supported in part by the National Institutes of Health (NIH) under Grant EB006615.

[†] Corresponding author

tissue behavior under different deformation modes and large strain. The rest of the paper is organized as follows. In section II, we describe the materials and methods used to conduct the experiments as well as modeling of liver tissue under tension, compression, and pure shear. In section III, we present the results from our experimental work and theoretical model. Finally, in section IV, we make some concluding remarks about our model.

II. MATERIALS AND METHODS

A. Ex-vivo Experiments of Pig Liver Tissue

1) Specimen preparation

For each test all tissue samples were cut from frozen porcine liver and remained frozen until the time of the test. Careful attention was given to the orientation of the tissue samples. The samples were extracted perpendicular to the liver top surface and tested in that direction. Samples with large blood vessels or obvious pores were discarded. There are several reasons for us to test frozen-thawed tissue. Besides the obvious convenience for storage, an important requirement is to be able to cut the sample into the required shape and size while avoiding excessive pre-strain to the tissue when it is fresh (or thawed) and very soft. When the liver freezes, its volume increases due to high water content. Due to this expansion, the liver tissue is very likely to be in a simple and homogeneous stress state. Therefore by monitoring the shape change of the sample after thawing and considering the effect of gravity on the specimen, we can compute the zero stress state, which is necessary for modeling purposes. Freezing may be treated as one type of preconditioning. Its effect on the mechanical properties of spleen tissue has been shown to be negligible [7].

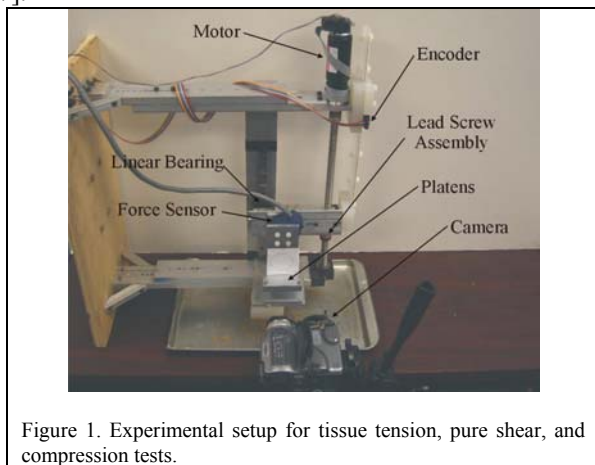


Figure 1. Experimental setup for tissue tension, pure shear, and compression tests.

Cylindrical samples of diameter 25.4 mm and height ~11 mm were cut for compression tests. The samples for pure shear and tension tests were cut into the shape of rectangular prisms. The original width and thickness of shear test samples was ~51 mm and ~11 mm respectively. The width and thickness of samples for tension test was ~17 mm and

~15 mm, respectively. All tests were performed at a constant velocity of 1.3 mm/s. The soft-tissue was not preconditioned prior to the experiments and only one loading was executed on each sample.

2) Experimental setup

A test apparatus (see Figure 1) has been designed and constructed to record force and displacement data for soft-tissue tension, compression, and pure shear tests. The equipment interacting with the tissue sample is attached to a JR3 6-axis force/torque sensor that allows measurement of vertical force in the range of 0.05 – 50N. The entire device is controlled via a dSPACE DS1103 controller board (dSPACE, Inc.) which also records the force and displacement data.

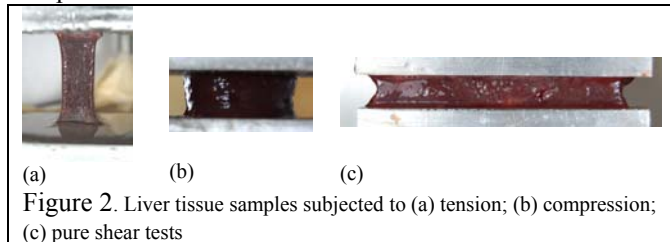


Figure 2. Liver tissue samples subjected to (a) tension; (b) compression; (c) pure shear tests

3) Experimental protocol

Tension: Tension tests were conducted by attaching two parallel plates to the experimental setup as seen in Figure 2. The top plate was rigidly mounted to the JR3 force sensor. The tension test utilized rectangular pieces of tissue that were adhered to the two parallel plates through the application of a thin layer of cyanoacrylate glue to each of the plates. The sample was fixed to the plates while frozen and allowed ample time to thaw while being sprayed with a mist of water. Upon completion of the thawing process tension was applied to each sample until the point where the glue failed and the tissue lifted from the plate. During the experiments, images were acquired via a Nikon D40 digital camera at 3 frames/s.

Unconfined compression: The setup for unconfined compression tests is almost identical to that of the tension test. During compression tests the plates are covered with a thin layer of petroleum jelly to minimize friction between the plates and the tissue. The tissue samples for the compression test are allowed to thaw in saran wrap prior to placement on the plates. This helps in maintaining the uniform shape of the sample prior to testing. During the test the sample moves a much shorter distance, so a digital video camera is used to obtain the image data for the test at much higher frame rate.

Pure shear: In pure shear test case two sets of vertical, serrated tissue clamps are used to hold the sample in the correct orientation. One set is connected to the JR3 force sensor while the other is fixed to the frame in a similar manner to the plates in the tension test. The clamps are comprised of two aluminum plates with 3 mm wide teeth which are rounded on the edges. These teeth provide the ability to maintain a firm grasp of the tissue without cutting through the sample. The sample is fixed between the two clamps while frozen and allowed to thaw under a mist of

water to maintain sample hydration. As the sample is stretched, force, displacement, and image data is recorded.

4) Strain measurement

The sequential images recorded during the experiments were analyzed and correlated to the force and displacement data to obtain the nominal stress vs. stretch ratio. For the tension and pure shear tests, the nature texture on the sample surface can be clearly seen (after spraying water mist before the test) during the entire loading process. Consequently, they are excellent markers for imaging. We used digital image correlation (DIC) technique to track these textures and calculate the strain field. For compression test, there is a loss of surface features as the tissue is compressed. Consequently, we have adopted the Canny edge detection algorithm to detect the boundary of the tissue and analyzed the deformation of the samples.

Since plates or specimen clamps create complicated states of stress and strain in the region surrounding the plate/clamp in the process of testing, non-contacting strain measurement techniques are needed to measure the strain on the specimen, but away from the plate/clamp, where a relative pure strain state is occurring. The use of DIC provides another benefit, namely, an accurate measure of the local strain in the region which is at zero strain state before the test. Since the tissue is very soft, it will deform by its own weight after thawed from frozen state. The result is that part of the sample near the top plate is in tension and the part near the bottom plate is in compression, so there is one region of the sample that is in the stress free state before external loading is applied. Therefore the local strain measured from a middle plane is indeed the accurate true strain, which is the deformation with respect to zero strain state. For compression test, the measured strain is corrected by a factor which is approximated by the ratio of height before and after sample thawing. From Figure 3, we can see the correction is just like a shift of the compression curve to the left. If we want more accurate estimation about the deformation caused by the weight, carefully designed experiments and simulations are needed. This is the topic of ongoing research in our group.

B. Theories for modeling of liver tissue

The length scale considered in a liver surgical simulation is roughly between 200mm and 0.2mm (roughly the thickness of blade or diameter of needle), which is equal or less than the organ size and larger than the micro-structure dimensions. For this length scale, it is reasonable to treat the liver as continuum tissue [14] with some macro-scale ducts inside and enclosed by capsule[6, 15]. Because of the uniform histology of liver tissue across species and its high water content, we can consider it to be isotropic, homogeneous and incompressible. If we assume the existence of a strain energy function and exclude the strain rate effect, the mechanical response of such materials can be described by a hyper-elastic model.

1) Hyper-elastic strain energy functions for isotropic incompressible material

Let \mathbf{X} be the coordinate of a material point in the reference configuration and \mathbf{x} its coordinate in the current configuration. The deformation gradient is given by

$$\mathbf{F} = \frac{\partial \mathbf{x}}{\partial \mathbf{X}} \quad (1)$$

The right Cauchy-Green deformation tensor, \mathbf{C} , is defined as

$$\mathbf{C} = \mathbf{F}^T \mathbf{F} \quad (2)$$

The symmetric tensor \mathbf{C} is positive definite, by the spectral theorem[16], we have:

$$\mathbf{C} = \sum_{A=1}^3 \lambda_A^2 \mathbf{N}^{(A)} \otimes \mathbf{N}^{(A)}, \quad \|\mathbf{N}^{(A)}\| = 1 \quad (3)$$

where $\mathbf{N}^{(A)}$ is eigenvectors of \mathbf{C} and $\lambda_A^2 > 0$ is the eigenvalue.

λ is also called principal stretch ratio. Relative to the zero-stress reference configuration, the state of strain can be completely specified by the three principal stretches and the directions of the principal axes of strain. When the material is incompressible the constraint equation is:

$$\det(\mathbf{F}) = \lambda_1 \lambda_2 \lambda_3 = 1 \quad (4)$$

which must be satisfied throughout the material.

a) *Polynomial form of strain energy:* For a isotropic, incompressible material, the strain energy function may be expressed as a function of strain invariants[17], given by:

$$I_1 = \text{trace}(\mathbf{C}) = \lambda_1^2 + \lambda_2^2 + \lambda_3^2 \quad (5)$$

$$I_2 = \frac{1}{2} [I_1^2 - \text{trace}(\mathbf{C}^2)] = \lambda_1^{-2} + \lambda_2^{-2} + \lambda_3^{-2}$$

The Mooney-Rivlin material is an example of a strain energy function with polynomial form of strain invariants I_1 and I_2 . Equation (6) is the two-constant version of the energy function for the Mooney-Rivlin material

$$W = \frac{C_1}{2} (I_1 - 3) + \frac{C_2}{2} (I_2 - 3) \quad (6)$$

where C_1 and C_2 are material constants, and $C_1, C_2 > 0$. The simplest polynomial based energy function is the neo-Hookean model (the case where $C_2=0$ in the Mooney-Rivlin model) and it is given by:

$$W = C_1 (I_1 - 3) \quad (7)$$

b) *Ogden form of strain energy:* Departing from the practice of writing the strain energy as a function of strain invariants I_1 and I_2 , Ogden [18] proposed a more general form of strain invariant for isotropic material,

$$I(\alpha) = \lambda_1^\alpha + \lambda_2^\alpha + \lambda_3^\alpha \quad (8)$$

where α is a real number, positive or negative. The Ogden form strain energy function can be written as:

$$W = \sum_k C_k (I(\alpha_k) - 3) = \sum_k C_k (\lambda_1^{\alpha_k} + \lambda_2^{\alpha_k} + \lambda_3^{\alpha_k} - 3) \quad (9)$$

where the C_k 's are constants and k is the number of terms included in the summation. Since $I(\alpha)$ is symmetric in

principal stretches λ_1 , λ_2 and λ_3 , the strain energy is also symmetric in the three principal stretches.

Compared with polynomial forms of models, Ogden's model is mathematically more simple and provides an accurate representation of the mechanical response of rubber-like material for a large range of deformations [18].

2) Hyper-elastic strain energy function for bio-tissues

In a typical single mode stress-strain curve of bio-tissues, the initial low-stiffness toe region is followed by a region of higher stiffness. In order to represent this type of mechanical response, exponential or logarithmic functions were used. Exponential form of strain energy functions were proposed by Fung and used in [7], and [8] to model spleen and liver tissues. A general form of exponential strain energy function can be written as [12]:

$$W = C_1(e^{C_2(I_1-3)} - 1) + C_3(I_2 - 3) \quad (10)$$

A combined logarithmic and polynomial form of strain energy is proposed by Chui et al [12],

$$W = -C_1 \ln(1 - C_2(I_1 - 3)) + C_3(I_1 - 3) \quad (11)$$

Both strain energy functions would be good enough if only single mode of deformation, i.e., compression or tension, is present. The above functions were also used to model liver tissue in combined compression and elongation experiments [12]. However, for some soft tissues which demonstrate short toe region in compression and extended toe region in tension, as shown in our experimental results, the strain energy functions in (10) and (11) are not capable of representing this behavior.

3) Combined logarithmic/exponential and Ogden strain energy function for very soft bio-tissue

Ogden model is good in small strain range to represent multi-axial deformations of soft tissue, as demonstrated in [9] for brain tissue. In order to account for the sharp increase of stiffness after the toe region, exponential or logarithmic functions are needed in the strain energy functions. Equation (12) and (13) are our proposed combined energy functions for isotropic soft tissue material.

$$W = C_1[\exp(C_2(\lambda_1^{\alpha_1} + \lambda_2^{\alpha_1} + \lambda_3^{\alpha_1} - 3)) - 1] + C_3(\lambda_1^{\alpha_2} + \lambda_2^{\alpha_2} + \lambda_3^{\alpha_2} - 3) \quad (12)$$

$$W = -C_1 \ln(1 - C_2(\lambda_1^{\alpha_1} + \lambda_2^{\alpha_1} + \lambda_3^{\alpha_1} - 3)) + C_3(\lambda_1^{\alpha_2} + \lambda_2^{\alpha_2} + \lambda_3^{\alpha_2} - 3) \quad (13)$$

where C_1 , C_2 , C_3 , α_1 and α_2 are material constants to be determined by comparison of theory and experiment.

4) Constitutive equations for combined logarithmic and Ogden model

For incompressible material, the principal Cauchy stresses can be determined from

$$\sigma_i = \lambda_i \frac{\partial W}{\partial \lambda_i} - p \quad (i = 1, 2, 3) \quad (14)$$

Because the material is incompressible, the hydrostatic pressure p is decoupled from the deformation and has to be calculated directly from the equilibrium equations.

Substituting (13) into (14), we have the principal Cauchy stresses for combined logarithmic and Ogden model as:

$$\sigma_i = \frac{C_1 C_2 \alpha_1 \lambda_i^{\alpha_1}}{1 - C_2(\lambda_1^{\alpha_1} + \lambda_2^{\alpha_1} + \lambda_3^{\alpha_1} - 3)} + C_3 \alpha_2 \lambda_i^{\alpha_2} - p \quad (15)$$

a) *Uniaxial tension and compression*: Let $\lambda_1 = \lambda$ be the stretch ratio in the direction of tension or compression, and $\sigma_1 = \sigma$ the corresponding principal Cauchy stress. The other two principal stresses are assumed to be zero, since no lateral forces are applied in the experiment. Because the material is incompressible, we have: $\lambda_2 = \lambda_3 = \lambda^{-\frac{1}{2}}$. The stress can be expressed as:

$$\sigma = \frac{C_1 C_2 \alpha_1 \lambda^{\alpha_1}}{1 - C_2(\lambda^{\alpha_1} + 2\lambda^{-\frac{\alpha_1}{2}} - 3)} + C_3 \alpha_2 \lambda^{\alpha_2} - p \quad (16)$$

and

$$0 = \frac{C_1 C_2 \alpha_1 \lambda^{-\frac{\alpha_1}{2}}}{1 - C_2(\lambda^{\alpha_1} + 2\lambda^{-\frac{\alpha_1}{2}} - 3)} + C_3 \alpha_2 \lambda^{-\frac{\alpha_2}{2}} - p \quad (17)$$

Elimination of p from (16) and (17) yields

$$\sigma = \frac{C_1 C_2 \alpha_1 (\lambda^{\alpha_1} - \lambda^{-\frac{\alpha_1}{2}})}{1 - C_2(\lambda^{\alpha_1} + 2\lambda^{-\frac{\alpha_1}{2}} - 3)} + C_3 \alpha_2 (\lambda^{\alpha_2} - \lambda^{-\frac{\alpha_2}{2}}) \quad (18)$$

The nominal stress (defined as force per unit unstrained area of cross-section), is given by:

$$T = \sigma \lambda^{-1} = \frac{C_1 C_2 \alpha_1 (\lambda^{\alpha_1-1} - \lambda^{-\frac{\alpha_1-1}{2}})}{1 - C_2(\lambda^{\alpha_1} + 2\lambda^{-\frac{\alpha_1}{2}} - 3)} + C_3 \alpha_2 (\lambda^{\alpha_2-1} - \lambda^{-\frac{\alpha_2-1}{2}}) \quad (19)$$

b) *Pure shear*: In pure shear one of the principal stretch ratio is held fixed, $\lambda_2=1$, say. Setting $\lambda_1 = \lambda$ and $\lambda_3 = \lambda^{-1}$, the stress-strain relations (15) reduces to:

$$\sigma_1 = \frac{C_1 C_2 \alpha_1 \lambda^{\alpha_1}}{1 - C_2(\lambda^{\alpha_1} + \lambda^{-\alpha_1} - 2)} + C_3 \alpha_2 \lambda^{\alpha_2} - p \quad (20)$$

and

$$0 = \frac{C_1 C_2 \alpha_1 \lambda^{-\alpha_1}}{1 - C_2(\lambda^{\alpha_1} + \lambda^{-\alpha_1} - 2)} + C_3 \alpha_2 \lambda^{-\alpha_2} - p \quad (21)$$

The force per unit undeformed area of cross-section in the direction of extension is thus given by:

$$T = \sigma_1 \lambda^{-1} = \frac{C_1 C_2 \alpha_1 (\lambda^{\alpha_1-1} - \lambda^{-\alpha_1-1})}{1 - C_2(\lambda^{\alpha_1} + \lambda^{-\alpha_1} - 2)} + C_3 \alpha_2 (\lambda^{\alpha_2-1} - \lambda^{-\alpha_2-1}) \quad (22)$$

III. RESULTS AND DISCUSSION

A. Experimental results

Figure 3 shows the nominal stress vs. the stretch ratio in the loading direction for all three types of tests. The results of two experiments are shown for each test. These preliminary results are not sufficient for proper statistical analysis, but allow a first insight on estimating the local mechanical properties of soft-tissue. All of the stress vs. stretch ratio curves have similar shape, i.e., little resistance is offered to loading at low stretch ratio (toe region), but at larger stretch ratios, the material stiffens dramatically. Since the curves for simple tension finish at the place where the glue fail, we can't see the response of tissue at high tensile stress, but the trend of the rapid increase of stress can be seen in Figure 3.

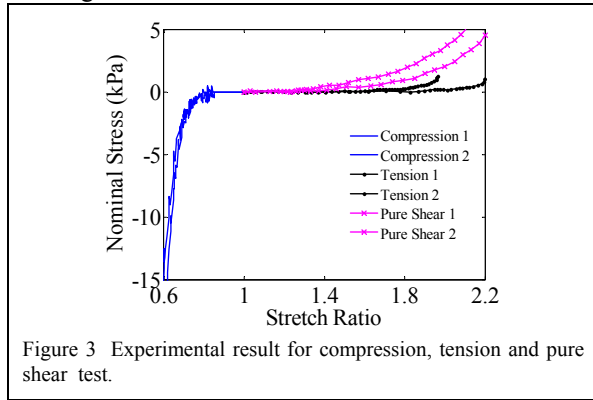


Figure 3 Experimental result for compression, tension and pure shear test.

The toe region of stress-stretch curve for tension is significantly longer than that for compression. Similar result for brain tissue is reported in [9]. This extended toe region for tension is different from that reported in [12]. There are two reasons that could contribute to the difference: 1) the preconditioning is different. Fung [13] reported that different preconditioning will result in different mechanical response for bio-tissue. We did no preconditioning except freezing the liver, and 2) the zero strain states are defined differently.

B. Theoretical analysis

In this paper, we are not trying to get the best fit of the experimental data using some optimization algorithm. Instead, the purpose of this section is to demonstrate the ability of the new model to fit the experimental data. We also present the following method, which can fit the exact length of toe regions for both tension and compression tests.

From Figure 3, we can see that the stiffness increases sharply at $\lambda \approx 0.65$ and $\lambda \approx 2.1$ for compression and tension, respectively. In (19) it is the following part of the equation,

$$f(\lambda) = C_2(\lambda^{\alpha_1} + 2\lambda^{\frac{-\alpha_1}{2}} - 3) \quad (23)$$

that decides the length of the toe region. Therefore, we can assume that stress is approaching infinity at $\lambda = 0.61$ and $\lambda = 2.15$ by forcing the following conditions:

$$f(0.61) = C_2(0.61^{\alpha_1} + 2 \times 0.61^{\frac{-\alpha_1}{2}} - 3) = 1 \quad (24)$$

$$f(2.15) = C_2(2.15^{\alpha_1} + 2 \times 2.15^{\frac{-\alpha_1}{2}} - 3) = 1 \quad (25)$$

Consequently, by solving (24) and (25), we get:

$$\alpha_1 = -6.0122, \quad C_2 = 0.05889 \quad (26)$$

The rest of the material constants can be determined by comparing the experimental results with those calculated from (19) and (22). The following material constants,

$$C_1 = 200; \quad C_3 = 2.5; \quad \alpha_2 = -8 \quad (27)$$

together with those in (26) were used to calculate stress-stretch curves, which is shown in Figure 4.

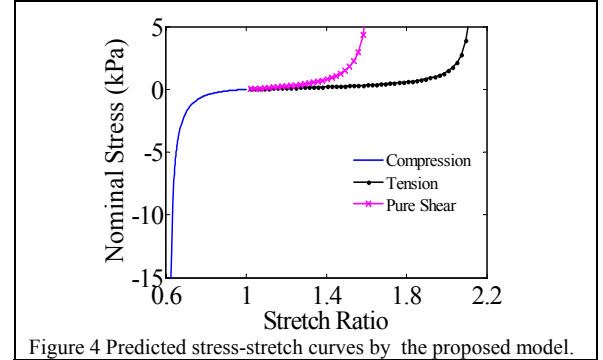


Figure 4 Predicted stress-stretch curves by the proposed model.

When $\lambda > 1.5$, the predicted pure shear nominal stress is much higher than that measured from experiments. In fact, the stress is approaching infinity around stretch ratio of 1.64. If $\alpha_1 < 0$ and $|\alpha_1| > 1$, it can be proved that calculated pure shear stress will increase rapidly around λ_c^{-1} , where λ_c is the set lower boundary of stretch ratio for compression. For real tissue, it is impossible to increase the stress that high. The microstructure of the tissue might start to break after a certain point. In experiments, we found that the tissue does not recover to its original length, if its deformation was larger than the toe region.

Overall, the predicted result is very good, considering there are only 5 material constants for the unified model. The fitting results can be improved by using some appropriate optimization. Similar result can be obtained by using the combined exponential and Ogden strain energy defined in (13).

Figure 5 and Figure 6 show the stress-strain curves fitted by using Ogden model and Chui's model, respectively. The result from the Ogden model is very good for compression and the tension toe region, but the stress increase after toe region is less sharp compared with that from our proposed model. Chui's model can only fit tension or compression data, but not both. The parameters for Ogden's model is obtained by using the provided function in ABAQUS to best fit one of the two sets of experimental data. The curves ($C_1 = 2.38 \times 10^{-6}$, $C_2 = 0.1699$, $\alpha_1 = 25$, $\alpha_2 = -16.63$) in Figure 5 are fitted from compression and tension data. The best fit results from 3 modes of deformation are not stable. The combined logarithmic and polynomial form of strain energy function as shown in Chui's model is a special case of our combined logarithmic and Ogden form strain energy with $\alpha_1 = 2$, and $\alpha_2 = 2$. Because there is only one

constant, C_2 , in function $f(\lambda)$, which can define the length of toe region for Chui's model, the bounds for tension and compression are coupled. Only one of them can be defined. In Figure 6, we can see this model can not fit both our tension and compression data. In Figure 6 curve 1, the parameters are: $C_1 = 60$, $C_2 = 1.55$, $C_3 = 100$. In Figure 6 curve 2, the parameters are: $C_1 = 60$, $C_2 = 0.45$, $C_3 = 200$.

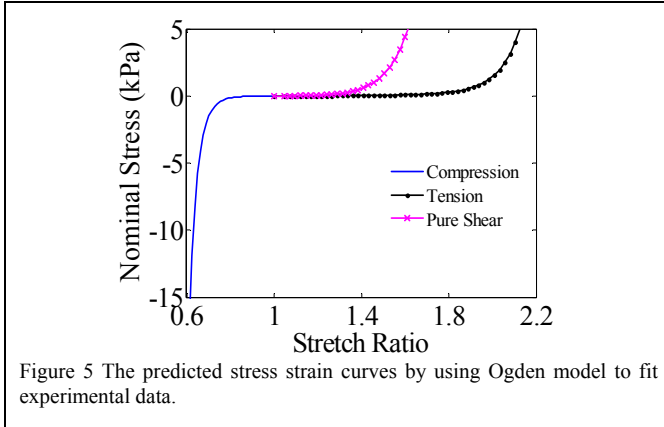


Figure 5 The predicted stress strain curves by using Ogden model to fit experimental data.

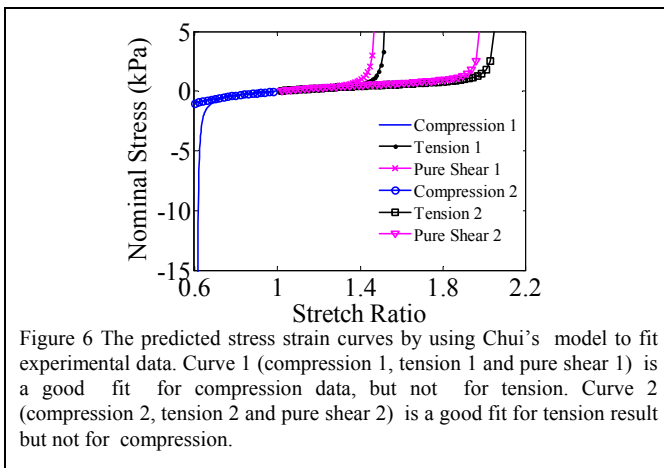


Figure 6 The predicted stress strain curves by using Chui's model to fit experimental data. Curve 1 (compression 1, tension 1 and pure shear 1) is a good fit for compression data, but not for tension. Curve 2 (compression 2, tension 2 and pure shear 2) is a good fit for tension result but not for compression.

IV. CONCLUSION

In this paper, we present results of simple tension, unconfined compression and pure shear tests for ex-vivo pig liver tissue in finite deformation. Digital image correlation and image processing technique were used to accurately measure the local strain. The results showed that liver tissue behavior in one deformation mode is considerably different from its behavior in other modes; therefore, tissue constitutive models based on only one type of experiments are not suitable for description of tissue behavior in general.

We developed a new constitutive model based on combined logarithmic and Ogden strain energy. This model is adequate to describe the full range of deformation for both compression and tension, and also good for low strain (<35%) deformation of pure shear. To the best of our knowledge, this is the first result of its kind. Though we only consider modeling liver tissue here, the strain energy function and the approach to determine its material

parameters are quite general and can be used for a wide variety of soft tissue modeling.

REFERENCES

- [1] K. Miller and K. Chinzei, "Constitutive modelling of brain tissue: experiment and theory," *J Biomech*, vol. 30, pp. 1115-21, Nov-Dec 1997.
- [2] M. Farshad, M. Barbezat, P. Flueler, F. Schmidlin, P. Graber, and P. Niederer, "Material Characterization of the Pig Kidney in Relation with the Biomechanical Analysis of Renal Trauma," *J. Biomechanics*, vol. 32, pp. 417-425, 1999.
- [3] T. Hu and J. P. Desai, "Modeling Large Deformation in Soft-tissues: Experimental results and Analysis," in *Eurohaptics*, Germany, 2004.
- [4] H. Saraf, K. T. Ramesh, A. M. Lennon, A. C. Merkle, and J. C. Roberts, "Measurement of the Dynamic Bulk and Shear Response of Soft Human Tissues," *Experimental Mechanics*, vol. 47, pp. 439-449, 2007.
- [5] A. E. Kerdok, M. P. Ottensmeyer, and R. D. Howe, "Effects of perfusion on the viscoelastic characteristics of liver," *Journal of Biomechanics*, vol. 39, pp. 2221-2231, 2006.
- [6] M. Hollenstein, A. Nava, D. Valtora, J. G. Snedeker, and E. Mazza, "Mechanical Characterization of the Liver Capsule and Parenchyma," in *Biomedical Simulation*. vol. 4072/2006, M. Harders and G. Szekely, Eds.: Springer Berlin / Heidelberg, 2006, pp. 150-158.
- [7] P. J. Davies, F. J. Carter, and A. Cuschieri, "Mathematical Modeling for Keyhole Surgery Simulations: A Biomechanical Model for Spleen Tissue," *IMA J. Applied Math*, vol. 67, pp. 41-67, 2002.
- [8] E. Roan and K. Vemaganti, "The nonlinear material properties of liver tissue determined from no-slip uniaxial compression experiments," *J Biomech Eng*, vol. 129, pp. 450-6, Jun 2007.
- [9] K. Miller and K. Chinzei, "Mechanical properties of brain tissue in tension," *J Biomech*, vol. 35, pp. 483-90, Apr 2002.
- [10] E. M. Alessandro Nava, Frederic Kleinermann, Nick J. Avis, John McClure, "Determination of the Mechanical Properties of Soft Human Tissues through Aspiration Experiments," in *Medical Image Computing and Computer-Assisted Intervention - MICCAI 2003*. vol. 2878: Springer Berlin / Heidelberg, 2003, pp. 222-229.
- [11] M. Kauer, "Inverse finite element characterization of soft tissues with aspiration experiments," in *Mechanical engineering*. vol. Doctor of technical science Zurich: Swiss federal institute of technology 2001, p. 143.
- [12] C. Chui, E. Kobayashi, X. Chen, T. Hisada, and I. Sakuma, "Combined compression and elongation experiments and non-linear modelling of liver tissue for surgical simulation," *Medical & Biological Engineering & Computing*, vol. 42, pp. 787-798, 2004.
- [13] Y. C. Fung, *Biomechanics: Mechanical properties of living tissues*, Second edition ed. New York: Springer-Verlag, 1993.
- [14] S. B. D. Stephen C. Cowin, *Tissue Mechanics*, 1st ed. New York: Springer Science+Business Media, LLC, 2007.
- [15] P. N. J.G. Snedeker, F.R. Schmidlin, M. Farshad, C.K. Demetropoulos, J.B. Lee, K.H. Yang, "Strain-rate dependent material properties of the porcine and human kidney capsule," *Journal of Biomechanics*, vol. 38, pp. 1011-1021, 2005.
- [16] R. L. T. J.C. Simo, "Quasi-incompressible finite elasticity in principal stretches, continuum basis and numerical algorithms," *Comput Method Appl M*, vol. 85, pp. 273-310, 1991.
- [17] E. H. Dill, *Continuum Mechanics: Elasticity, Plasticity, Viscoelasticity* Boca Raton, London, New York: CRC Press, 2006.
- [18] R. W. Ogden, "Large deformation isotropic elasticity - on the correlation of theory and experiment for incompressible rubberlike solids," *Proc. R. Soc. Lond. A.*, vol. 326, pp. 565-584, 1972.